nature sustainability

Article

https://doi.org/10.1038/s41893-023-01160-2

Biorenewable and circular polydiketoenamine plastics

Received: 15 December 2022

Accepted: 26 May 2023

Published online: 27 July 2023



Check for updates

Jeremy Demarteau 1, Benjamin Cousineau 1, Zilong Wang^{2,3,4,5}, Baishakhi Bose ⁵, Seokjung Cheong^{2,3,4,5}, Guangxu Lan ^{2,5}, Nawa R. Baral ^{2,5}, Simon J. Teat 6, Corinne D. Scown 2,5,7,8, Jay D. Keasling 4,3,4,5,9,10 & Brett A. Helms 1,2,11

Amid growing concerns over the human health and environmental impacts of plastic waste, the most promising solution would be to build a circular plastics economy where sustainability considerations dictate the full life cycle of plastics use including replacing petrochemicals with biorenewables. Here we show that by incorporating the polyketide triacetic acid lactone (TAL) in polydiketoenamines (PDK) we increase the working temperature of these circular plastics, opening the door wider to applications where circularity is urgently needed. By varying the number of carbons of TAL-derived monomers, both polymer properties and recycling efficiency are affected. Simply using glucose as the main carbon source, we engineered a process for producing bioTAL under fed-batch fermentation. A systems analysis of this bioprocess under different scenarios quantifies the environmental and economic benefits of PDK plastics and the risks when implemented at an industrial scale, providing opportunities in biorenewable circularity.

Bringing biorenewable circularity to plastics is critical to ensuring their sustainability¹⁻³. While bio-based monomers used to produce plastic resins are increasingly available from biomass and bioproducts^{1,4,5}, using them simply as drop-in replacements for commodity petrochemicals fails to deliver a bio-advantage in performance⁶. Justifying their use in plastics production therefore remains difficult, as they are often produced at higher cost than the petrochemical they seek to replace. Furthermore, few existing plastics, even if produced from bio-monomers, are chemically recycled in closed-loops, particularly monomer-to-monomer^{1,7}. Without biorenewable circularity, we will continue to consume the dwindling supply of fossil resources to meet the rapidly growing demand for plastics⁸; moreover, we will have few incentives to recover plastic waste for recycling and reuse, failing to meet our goals for sustainable manufacturing. Future generations of plastics should emphasize bio-advantaged designs that achieve high efficiency in chemical recycling with respect to monomer recovery at end of life^{6,9}, so that the biorenewable content may be recirculated across the maximum possible number of manufacturing cycles. If this was realized, there could be a confluence of performance, manufacturing and economic benefits to motivate the switch to new materials in the transition to a circular bio-plastics economy.

In support of this paradigm shift, we and others have demonstrated that circularity in emerging bio-plastics is achievable through codesign of polymers and chemical recycling processes (for example,

¹The Molecular Foundry, Lawrence Berkeley National Laboratory, Berkeley, CA, USA. ²Joint BioEnergy Institute, Emeryville, CA, USA. ³Department of Chemical and Biomolecular Engineering & Department of Bioengineering, University of California, Berkeley, CA, USA. 4QB3 Institute, University of California, Berkeley, CA, USA. ⁵Biological Systems and Engineering Division, Lawrence Berkeley National Laboratory, Berkeley, CA, USA. ⁶Advanced Light Source, Lawrence Berkeley National Laboratory, Berkeley, CA, USA. 7Energy Analysis and Environmental Impacts Division, Lawrence Berkeley National Laboratory, Berkeley, CA, USA. 8Energy & Biosciences Institute, University of California, Berkeley, CA, USA. Center for Synthetic Biochemistry, Shenzhen Institutes for Advanced Technologies, Shenzhen, People's Republic of China. 10 The Novo Nordisk Foundation Center for Biosustainability, Technical University Denmark, Kemitorvet, Kongens Lyngby, Denmark. 11 Materials Sciences Division, Lawrence Berkeley National Laboratory, Berkeley, CA, USA.

acidolysis, solvolysis, enzymolysis and catalytic ring-closing depolymerization)¹⁰⁻²⁸. Chen et al. have exploited ring-chain equilibria to enable circularity in polyesters and nylons from strained lactone and lactam monomers, some of which can be produced from bio-based raw materials¹³⁻¹⁵. Complementing these efforts. Mecking et al. have prioritized solvolysis in the deconstruction of polyesters and polycarbonates from high molecular weight diols and carboxylic acids¹⁰. Solvolysis and acidolysis are likewise applicable to bio-plastics featuring imine and diketoenamine bonds. Some of these bio-plastics have even shown properties similar to petroleum-derived plastics that remain difficult to recycle in closed-loops, such as polyethylene and polyurethane¹⁰. Among them, bio-plastics based on polydiketoenamines (PDK) stand out for the concomitantly high efficiency and low cost required to chemically recycle them to the same monomers used in primary resin production²³⁻²⁸. However, it remains a challenge to demonstrate circularity in bio-plastics while deriving benefits from their constituent bio-monomers.

Here we show that biorenewable circularity in plastics concomitantly delivers a useful bio-advantage by incorporating the polyketide triacetic acid lactone (TAL) in PDK, which are deconstructed to monomer at end of life with low carbon intensity in high yield and purity. The bio-advantage of TAL arises from its planarity, which promotes efficient stacking in the solid state and has the effect of densifying TAL-based PDKs (TAL-PDK). This densification raises the glass transition temperature (T_g) beyond a key threshold of 150 °C, making possible the use of TAL-PDKs in broader applications (for example, automotive)²⁹, where structural integrity up to that temperature is of great importance. To understand the prospects for producing PDK resins from TAL, we developed a fed-batch fermentation process for bioTAL production using an engineered strain of Escherichia coli that expresses a heterologous polyketoacyl-CoA thiolase, BktB, which converts acetyl-CoA into TAL in high titre. We also provide a detailed systems analysis of this process at different production volumes, where the environmental and economic benefits derived from biorenewability are quantified and delineated in the context of managing risk along the path to producing bioTAL and TAL-PDK resins at industrial scale.

Results

Biorenewable TAL-based PDK resins

PDK resins are prepared via spontaneous 'click' polycondensation reactions between polytopic triketone and amine monomers: no chemical condensation agent is required and water is the sole byproduct of the reaction^{23–28}. Triketone monomers used in PDK production are synthesized from various 1.3-diketones and diacids. During synthesis, acylation of the 1,3-diketone typically occurs first at oxygen, which is then followed by an O- to C-acyl rearrangement catalysed by 4-(dimethylamino)pyridine (DMAP)²⁶. Owing to structural similarities between O-acyl intermediates and the likely reactivity of the preferred tautomer of TAL, we hypothesized that TAL could stand in place of conventional petrochemical 1,3-diketones, such as dimedone, in monomer synthesis alongside common aliphatic C_{8-12} dicarboxylic acids (Fig. 1a) to make available biorenewable triketone monomers (TAL-TK 1-5) and in turn PDK resins (TAL-PDK 1-5). Confirming this hypothesis, TAL-TK 1–5 were prepared in 40–63% yield (after recrystallization) using N,N'-dicyclohexylcarbodiimide (DCC) and DMAP. We obtained single-crystal X-ray structures for TAL-TK 1, 3 and 5-all of which evidenced herringbone packing of the monomers in the solid state, due to stacking enabled by the planarity of TAL (Fig. 1b and Supplementary Figs. 1–2). This propensity for stacking and densification is highly differentiated from that exhibited by a similar triketone monomer prepared from the petrochemical dimedone, which is not planar (Supplementary Table 1). This difference in crystallinity is further exemplified in DSC analysis of TAL-TK monomers, showing sharp endothermic melting peaks for TAL-TK 1, 3 and 5 (150, 143 and 143 °C, respectively), while TAL-TK 2 and 4 shows broader transitions at lower temperatures (60 and 100 °C, respectively) (Supplementary Fig. 3). It follows that the properties of PDK resins produced from these triketone monomers may likewise have different properties arising from the unique microstructures afforded to each.

To understand these emergent microstructure–property relationships, we first prepared TAL-PDK resins 1–5 from TAL-TK monomers 1–5 and *tris*(2-aminoethyl)amine (TREN); as a control, we also prepared a PDK resin from TREN and a triketone monomer derived from dimedone. To confirm that the polycondensation was complete, we performed ¹³C solid-state nuclear magnetic resonance (NMR) spectroscopy on powdered samples of TAL-PDK 1–5 (Supplementary Figs. 4–8). We observed a disappearance of sharp peaks, otherwise corresponding to the crystalline triketone monomer, as well as a concomitant broadening of peaks corresponding to the polymer network. We further confirmed the extent of polymerization was high by powder X-ray diffraction, where sharp and intense peaks associated with the Bragg reflections of crystalline triketone monomers completely subsided to peaks exhibiting lower-intensity and significant broadening due to amorphization into a glassy vitrimer network (Supplementary Fig. 9).

Enabled by the intrinsic dynamic covalent character of vitrimers, crosslinked PDK resin powders remain thermally processable, for example, by compression moulding³⁰⁻³². For TAL-PDK resins 1-5, compression moulding at 20 kPsi pressure required temperatures of 150, 140, 130, 125 and 110 °C, respectively, to fabricate samples (Fig. 1c and Supplementary Fig. 10); thus, lowering vitrimer crosslinking density has the effect of lowering the energy requirement for PDK manufacturing. Whereas the expected colour and high transparency of the vitrimers were readily apparent for TAL-PDK 1, 3 and 5 (as well as the control), colours were unexpectedly darker and hazier for TAL-PDK 2 and 4. The natural hue of TAL-PDK resins, which varies with crosslinking density and odd-even effects, would need to be accounted for in compounding with pigments to arrive at desired specifications. Nonetheless, we observed a monotonic and well-behaved decrease in the glass transition temperature (T_g) with decreasing crosslinking density (Fig. 1d and Supplementary Fig. 11). Importantly, in all cases we found that TAL dramatically raises T_g when incorporated into PDK resins: for example, the T_g of biorenewable TAL-PDK 3 is 36 °C higher than that of the related dimedone petrochemical control ($T_g = 96$ °C), pointing to the key role of PDK microstructure on thermal properties. To provide context for thermal stability, thermal gravimetric analysis data of the different formulations, with monomers (TAL-TK 1-5), powder and pressed-moulded polymers (TAL-PDK 1–5) do not show any degradation below 200 °C (Supplementary Fig. 12). Structural integrity of glassy polymer networks is critical for most commercial applications, from automotive to protective barriers and sporting gear; increasing T_g to meet product specifications remains an outstanding challenge, yet appears addressable with TAL-based PDK resins on account of their unique microstructure.

Motivated by this bio-advantage and its link to polymer microstructure, we carried out further studies of PDK properties, where microstructure often dictates outcomes, including density (ρ) and storage modulus (E') at temperatures above T_g . For elastic polymer networks, E' is proportional to ρ as well as the crosslinking density. Absent significant changes to ρ (which are rare), E' should decrease monotonically with decreasing crosslinking density, as was observed for T_g ; however, that is not what we observed experimentally. Instead, we observed odd-even effects in both ρ and E', depending on the length of the diacid incorporated into the TAL-derived triketone monomer (Fig. 1e,f and Supplementary Fig. 13). In all cases, ρ and E' were higher for TAL-PDK materials than those of the related dimedone petrochemical control (Supplementary Tables 2 and 3), consistent with the body of evidence presented herein, indicating more efficient packing in the solid state and useful gains in elasticity and stiffness. For example, ρ is 1.078 g cm⁻³ and E' is 13.5 MPa for TAL-PDK 3, whereas ρ is 0.987 g cm⁻³ and E' is only 3.5 MPa for the control (that is, 3.9-fold lower than TAL-PDK 3).

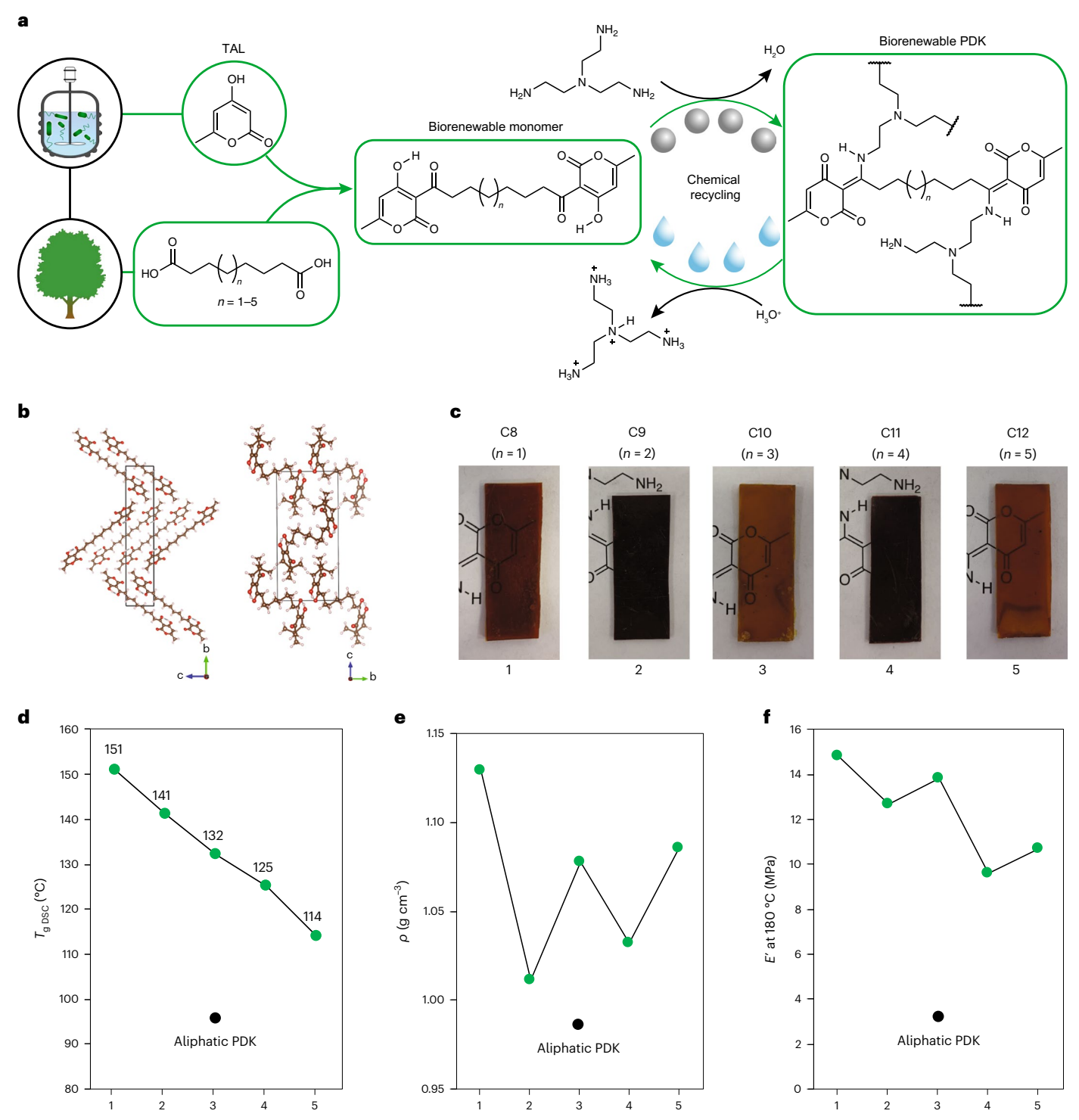


Fig. 1 | **Biorenewable circularity in PDK plastics derived from TAL. a**, Synthesis and chemical recycling of biorenewable PDK resins derived from TAL (TAL-PDK 1–5). **b**, Single-crystal X-ray structures of triketone TAL-TK 3 (left) and a related aliphatic triketone prepared from the petrochemical dimedone in place of TAL (right). **c**, Compression-moulded samples of TAL-PDK 1–5. **d**, Glass transition

temperatures ($T_{\rm g}$) measured by DSC ($T_{\rm gDSC}$) for TAL-PDK 1–5 and a related aliphatic PDK resin prepared from dimedone. **e,f**, Density (**e**) and storage modulus (**f**) (at rubbery state, 180 °C) of compression-moulded TAL-PDK 1–5 and a related aliphatic PDK prepared from dimedone.

We are unaware of previous reports of odd–even effects in vitrimer microstructure–property relationships, yet they appear intrinsic and relevant to their design for function. Until now, odd–even effects in elastic polymer networks had only been explored theoretically–for example, with respect to monomer topology, accounting for number of networking functionality in the monomers³³. Now, molecular

configuration of constituent monomers and their influence on polymer chain conformation within the network architecture emerge as further points of interest and intrigue. Although unrelated, given the dissimilarity between linear and crosslinked polymer architectures, these observations are nonetheless reminiscent of odd–even effects in thermal properties of thermoplastics—for example, the melting

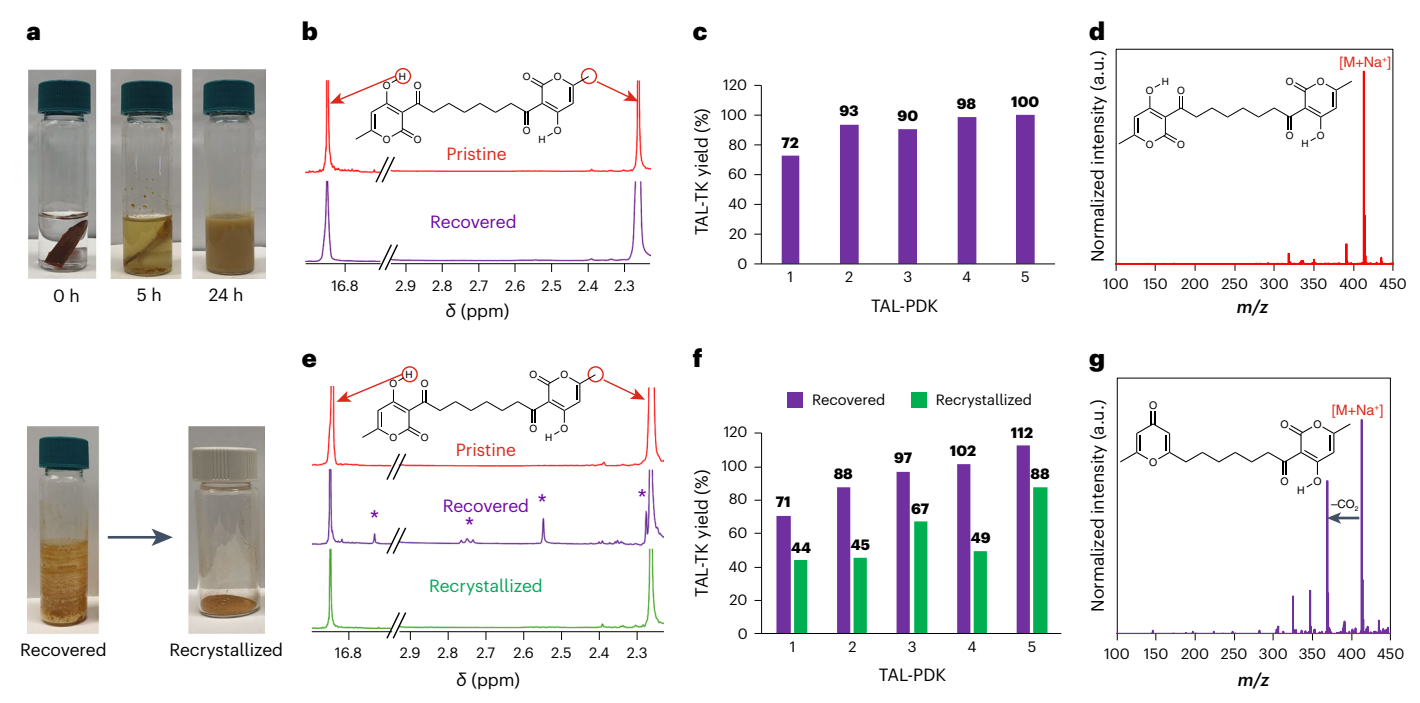


Fig. 2 | **Recycling of TAL-PDK formulations. a**, Acid-catalysed depolymerization of TAL-PDK 1 plastic and recovery of TAL-TK1 monomer. **b**, ¹H NMR spectra of pristine TAL-TK1 (top) along with crude TAL-TK1 recovered from chemically recycled TAL-PDK 1 resin (bottom). **c**, TAK-TK yields after acidolysis of TAL-PDK resins. **d**, ESI-MS spectrum of TAL-TK1. **e**, ¹H NMR spectra of pristine TAL-TK1 (top), crude TAL-TK1 recovered after acidolysis of thermally processed TAL-PDK

 $1 (middle) \ and \ TAL-TK1 \ recovered \ from \ the \ crude \ after \ recrystallization \ in \ EtOH \ (bottom). \ Characteristic peaks in the \ ^1H \ NMR \ spectra \ for \ important \ structural \ motifs \ are \ highlighted \ with \ red \ arrows, \ while \ impurities \ are \ identified \ by \ using \ purple \ asterisks. \ f, \ TAL-TK \ yields \ for \ both \ crude \ (purple) \ and \ recrystallized \ (green) \ monomers \ after \ acidolysis \ of \ TAL-PDK \ plastics. \ g, \ ESI-MS \ spectrum \ of \ crude \ TAL-TK1 \ recovered \ after \ acidolysis \ of \ thermally \ processed \ TAK-PDK1.$

points of 1,*n*-nylons³⁴. Odd–even effects, observed here in TAL-PDK materials, may be universal for polymer networks. In this way, we continue to unravel the foundations of thermoplastic-like character of vitrimers^{30–32}, including biorenewable PDK resins produced from TAL.

Molecular basis for TAL-PDK circularity in recycling

PDK resins typically undergo deconstruction to triketone and amine monomers in strong acid at ambient temperature. Unlike triketone monomers derived from dimedone (that is, the control), which have no cleavable linkages, those derived from TAL have motifs, such as the lactone, that may be susceptible to acidolysis. If lactone acidolysis is competitive with diketoenamine hydrolysis, then it could affect the materials efficiency of chemically recycling TAL-PDK resins back to monomer—for example, if products other than TK 1–5 are also generated. To quantify the efficiency of circularity for TAL-PDK 1-5, we carried out their acidolysis in 5 M HCl for 24 h, after which all deconstructed to dispersed solids of TAL-TK 1-5, along with ionized TREN, which remained ionized in solution (Fig. 2a). We isolated TAL-TK 1–5 solids in 72, 93, 90, 98 and 100% yield, respectively (Fig. 2c); TREN can be recovered separately in high purity from the aqueous phase using a basic ion exchange resin²³. Recycled TAL-TK 1-5 were indistinguishable from the pristine monomers by ¹H NMR spectroscopy (Fig. 2b and Supplementary Figs. 14-18), indicating that the TAL-TK motif is remarkably stable under these conditions. Furthermore, when compared to yields and purity for monomer recovery for dimedone-based PDK resins (that is, derived from petrochemicals), TAL-PDK circularity compares favourably, particularly for resins with lower crosslinking density.

In quantifying further the efficiency of TAL-PDK circularity in compression-moulded samples, we likewise found that lowering the crosslinking density was useful for ensuring high monomer recovery from TAL-PDK resins that had undergone conversion to various

form-factors at high pressure and temperature (Fig. 2e,f and Supplementary Figs. 19-32). Polymer degradation during thermal processing during manufacturing or even mechanical recycling at end of life can be detrimental towards the development of circular plastics. An analysis of the degradation products formed after thermal processing can be informative towards an improved understanding of vulnerable structures and degradation pathways. These insights may provide new design criteria for constructing PDKs and other circular materials. To this end, we analysed mass spectra for all crude triketones obtained after TAL-PDK deconstruction and compared these data with spectra obtained from the pristine monomers. In all cases, we observed a new and unique peak around 44 mass units below the peak corresponding to a [TAL-TK + Na]⁺ion (Fig. 2d,g and Supplementary Figs. 28–32). This indicated a loss of carbon dioxide from some monomers recovered after depolymerization. In parallel, we observed new yet minor peaks (<15%) in the δ = 6.7–17.0 ppm region of the ¹H NMR spectra for crude triketones. This indicated that while one triketone motif in the ditopic monomer remained intact in the minor byproduct of depolymerization reaction, the other had undergone decarboxylation during thermal processing (Supplementary Figs. 19-27). To remain consistent with the structural analysis afforded by mass spectrometry, it is likely that this transformation generates a y-pyrone. In cases where processing at high temperature and pressure led to materials degradation, we found triketone recrystallization from ethanol quite effective at removing unwanted γ -pyrone byproducts. Even with this additional purification process in place, TAL-TK 5 yields as high as 88% could be maintained, whereas in the absence of thermal processing and recrystallization, 100% yields were obtained. This understanding of the molecular basis for biorenewable circularity with TAL-PDK materials elevates future designs that benefit from lower crosslinking density to minimize mechanochemical activation of susceptible bonds within the TAL-PDK network.

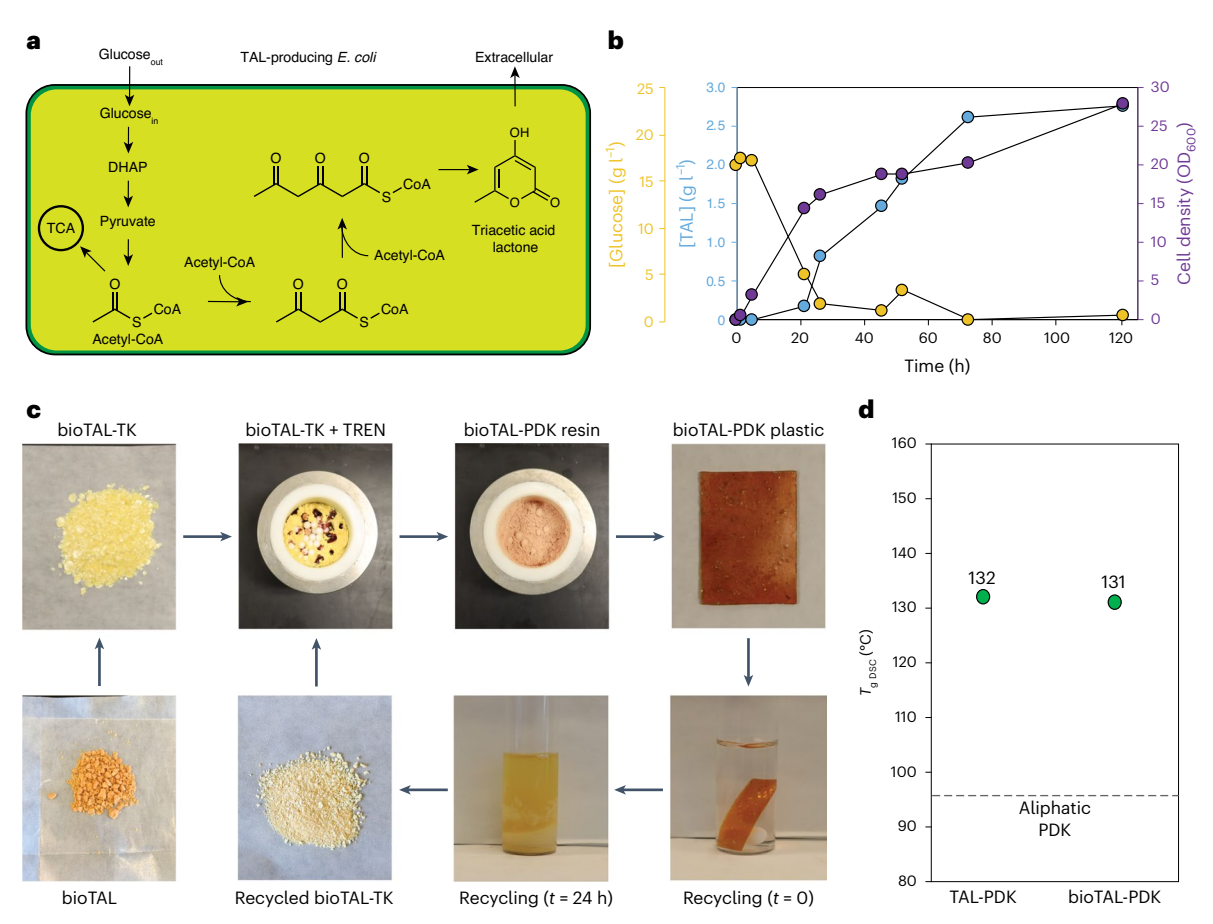


Fig. 3 | Biosynthesis of triacetic acid lactone (bioTAL) and biorenewable TAL-PDK characterization. a, Metabolic pathway for TAL biosynthesis in engineered $\it E. coli$ JBEI-3695. b, Cell growth (OD $_{600}$), TAL titre and glucose concentration in the 1-I fed-batch fermentation using $\it E. coli$ JBEI-3695 pBbASA-BktB. c, Closed-loop production and chemical recycling of biorenewable TAL-PDK 3. d, Comparison

of glass transition temperatures for petrochemical and biorenewable TAL-PDK 3, as well as a similar aliphatic PDK material produced from dimedone in place of BioTAL. Abbreviations: TCA, tricarboxylic acid cycle; DHAP, dihydroxyacetone phosphate.

Bioproduction of TAL

Polyketide natural products are ubiquitous: some serve as important medicines and others as useful chemicals or feedstocks for materials³⁵. TAL can be produced by the enzyme 2-pyrone synthase (2-PS), which catalyses a succession of decarboxylative Claisen condensation reactions. TAL bioproduction with 2-PS has been achieved in Yarrowia lipolytica (36 g l⁻¹) and Rhodotorula toruloides (28 g l⁻¹), although overall yields from common carbon sources, such as glucose, could be improved if TAL synthases that perform non-decarboxylative Claisen condensation using acetyl-CoA as a substrate were used rather than those that perform decarboxylative condensation using malonyl-CoA as a substrate³⁶⁻³⁸. Here we used the non-decarboxylative polyketoacyl-CoA thiolase, BktB³⁹, for TAL bioproduction in an engineered strain, E. coli JBEI-3695 (Fig. 3a). If successful, the advance could open the door to directly converting sugars from plant biomass hydrolysates to this valuable bioproduct in high yield⁴⁰, closer to bringing biorenewable circularity to PDK resins.

We synthesized the gene encoding BktB from <code>Burkholderia sp.</code> RF2-non_BP3 with codon-optimization for <code>E. coli</code> and cloned it into the vector pBbA5A, followed by transformation into <code>E. coli</code> JBEI-3695, which had some of its mixed-acid production enzyme genes deleted ($\Delta adhE \Delta ldhA \Delta frdBC \Delta pta$) to enhance TAL production. We performed growth and production in a 1-l fed-batch bioreactor with optimized production media (Supplementary Table 7), using glucose as the main carbon source. We monitored cell growth using optical density at 600 nm (OD600) of 1-ml cell samples removed periodically during the

production. The cells achieved a final OD₆₀₀ of 27.9 in 120 h and produced TAL to a final titre of 2.77 g l⁻¹ (Fig. 3b). The overall yield of TAL was around 0.11 g TAL per g of glucose, and the overall production rate was $0.035 \,\mathrm{g}\,\mathrm{l}^{-1}\mathrm{h}^{-1}$. This experiment was repeated to produce additional TAL batches for bioTAL-PDK synthesis (Supplementary Fig. 34). Although unoptimized, these results compare favourably to previous TAL yields from mixed carbon sources (glucose, fructose, sucrose and acetate) in Rhodotorula toruloides by 2-PS (0.089 g TAL per g of mixed carbon sources)41,42. After production and lyophilization of the broth, we extracted the mixture with ethyl acetate and isolated the desired TAL bioproduct (bioTAL) in high purity (Supplementary Fig. 35). We then synthesized a biorenewable triketone monomer bioTAL-TK 3 from bioTAL and sebacic acid, which we obtained as a bioproduct from Arkema (Fig. 3c). These 100% biorenewable triketone monomers showed essentially identical properties when used in the synthesis and chemical recycling of bioTAL-PDK 3 resins (Fig. 3d).

LCA and TEA of TAL bioproduction

To understand the key cost and greenhouse gas (GHG) emissions drivers of bioTAL production, we carried out a system-level techno-economic analysis (TEA) and life cycle GHG inventory. All costs and emissions estimates are based on the system summarized in Fig. 4a. We modelled a biorefinery where corn stover is pretreated with a bio-compatible ionic liquid (choliniumlysinate), followed by enzymatic hydrolysis, to generate a hydrolysate, which can be converted to bioTAL via bioconversion of both pentose and hexose sugars in engineered *E. coli* expressing

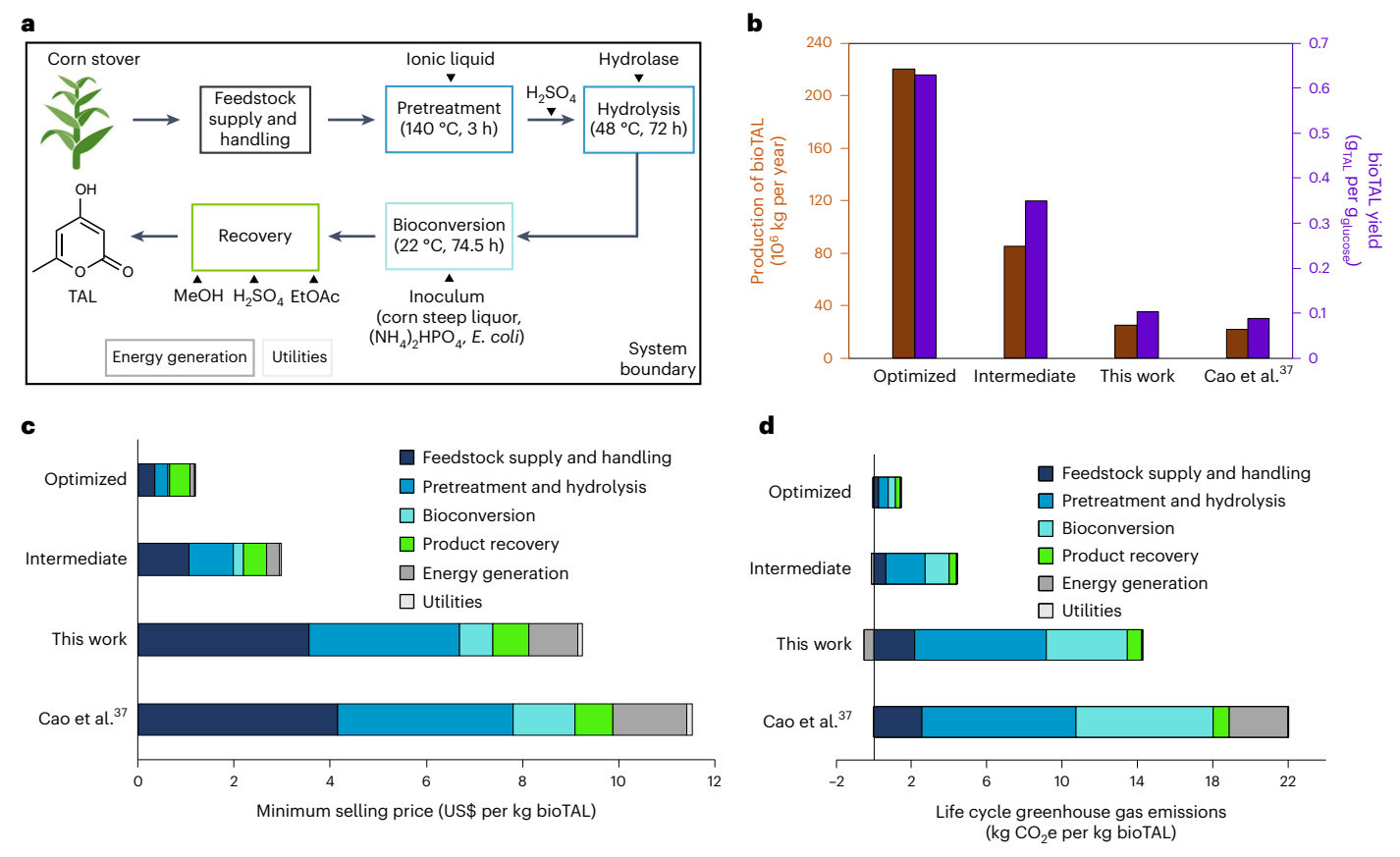


Fig. 4 | **Systems analysis of the production of bioTAL. a**, Simplified schematic system boundary. **b**, bioTAL annual production and yield under four different scenarios, adjusting for factors such as the product yield (Cao et al.: 12.7% of theoretical maximum³⁷: this work: 14.9% of theoretical maximum: intermediate:

50% of theoretical maximum; and optimized: 90% of theoretical maximum) and projected efficiencies gained at industrial scale. **c**,**d**, MSP (**c**) and life cycle GHG emissions (**d**) for bioTAL production across all four scenarios.

the non-native BktB thiolase. The cost of production is captured by a single metric minimum selling price (MSP). MSP refers to the product selling price at which the net present value of the project equals zero, after incorporating an internal rate of return (10% for this study). In other words, the MSP is the minimum price a company must sell the product for to be as profitable as their next best investment option. To estimate the MSP and generate mass and energy balances, we used a combination of experimental data and chemical process modelling to design and simulate a hypothetical commercial-scale bioTAL production facility. All process simulation was conducted in a commercial process modelling software package (SuperPro Designer-V12)⁴³. We translated outputs from the process model, including equipment sizing and costs, operating inputs and waste processing costs, into a separate cash flow model to determine the MSP of bioTAL.

To understand the impact of bioTAL yield and other process parameters on MSP, we analysed four biomass-derived bioTAL production scenarios based on the current demonstrated and future optimized yields. The scenario associated with 'this work' reflects the bioTAL yield experimentally demonstrated in this study with glucose, extrapolated to xylose assuming a commercial-scale biorefinery would use a cofermenting host. For comparison, we also considered a scenario built from the bioTAL yield in *R. toruloides* using 2-PS, as reported by Cao et al.³⁷ (Fig. 4b). The 'intermediate' scenario extrapolates from this study with a moderate improvement upon the current bioTAL yield, reaching approximately 50% of the theoretical maximum (0.35 g bioTAL per g of glucose, 0.315 g bioTAL per g of xylose). Both 'this work' and 'intermediate' scenarios rely on a bioconversion residence time of approximately 75 h. An 'optimized' scenario represents a mature

facility in which the bioTAL yield reaches approximately 90% of theoretical maximum (0.63 g bioTAL per g of glucose, 0.567 g bioTAL per g of xylose) and all process parameters have been optimized to reach a practical minimum production cost, including a reduction in residence time to 48 h. Material balances for the intermediate scenario and major costs and revenues associated with bioTAL production are presented in Supplementary Tables 8 and 9, respectively.

In biorenewable PDK production, bioTAL serves as a replacement to dimedone, a petrochemical priced at US\$10 per kg (ref. 44). As shown in Fig. 4c, all three scenarios tied to bioTAL production in E. coli using non-native BktB enzymes result in a lower MSP than the reported price for dimedone, whereas MSP is higher for the previously reported bioTAL production using 2-PS in R. toruloides. This encouraging result suggests that, provided the microbial host can be engineered to co-utilize both pentose and hexose sugars at comparable yields and rates, commercial-scale bioTAL production from corn stover can be cost-competitive with dimedone in the near term. The MSP results for the 'optimized' scenario of approximately US\$2 per kg of bioTAL represent a practical minimum and can be useful in screening for other applications where bioTAL may or may not compete with incumbent molecules. This optimized scenario can be viewed as something akin to a theoretical minimum; it is unlikely that costs could be reduced beyond that level. This exercise is useful because, if the optimized scenario was to result in higher costs than the petrochemical alternative (dimedone), this might suggest that bio TAL is not a viable replacement. For context, the prices of HDPE, PU and PET were US\$2.3 per kg, US\$4 per kg and US\$1.2 per kg, respectively⁴⁵. Using the optimized scenario, replacing dimedone with bioTAL would result in a cost lower than the previously

published PDK cost²⁶. Improvements across all aspects of the production system, including lower-cost corn stover, improved sugar yields, higher ionic liquid recovery rates, and increases in titre, rate and yield are needed to reach this ambitious target. In the near term, further research can improve the bioTAL recovery process (for example, bioTAL refinement via recrystallization, instead of chromatography), which will improve both the costs and energy use.

The life cycle GHG assessment is based on a cradle-to-gate system boundary and the functional unit is defined as one kg of bioTAL produced. We obtained life cycle inventory data and characterization factors for input materials and commodity polymers from peer-reviewed $literature {}^{25,46,47}, and LCA \, databases \, including \, ecoinvent {}^{48}, US \, Life \, Cycle \,$ Inventory (USLCI)⁴⁹, GREET⁵⁰ and WARM⁵¹ models. The GHG emissions footprint for dimedone has been reported to be 0.7–15 kg CO₂e per kg of dimedone in previous works²⁶. To contextualize our results, we use a median value of 8 kg CO₂e per kg of dimedone. The intermediate and optimized scenarios in Fig. 4d result in lower GHG emissions compared to dimedone. This result is encouraging, as it suggests that even with moderate improvement in current bioTAL yield for the intermediate scenario, keeping all other assumptions constant, commercial-scale bioTAL production from corn stover can result in lower GHG emissions when compared to dimedone in the near term. GHG emissions are higher for the previously reported bioTAL production using 2-PS in R. toruloides, when compared to dimedone. For 'this work' scenario, we found that GHG emissions were 1.7 times higher than the median value, and approximately equal to the highest reported value of dimedone.

Lower product yields and long bioconversion residence times translate into higher energy use, which drives GHG emissions. If lignin recovered from biomass is sufficient to meet the facility's heat and electricity demands, no fossil fuels are directly required. Any excess electricity can be sold to the grid (Supplementary Table 10); we assume these exports offset the US average grid mix. If lignin is not sufficient, supplemental natural gas is required for on-site combined heat and power generation. We found for the bioTAL production reported in 'this work' scenario that the pretreatment process is the single largest contributor to life cycle GHG emissions (51%), followed by bioconversion (31%). Switching to non-fossil energy sources could drive down the GHG footprint. Another opportunity for GHG emissions reduction would be to improve the solvent recovery rate. We assume 95% solvent recovery (ethyl acetate, methanol), which is readily achieved at industrial scale.

Discussion

Our summary findings show that biorenewable circularity with TAL-PDK is most promising when: bioprocesses for TAL production can be incorporated into lignocellulosic biorefineries that take in crop residues and other sustainable biomass feedstocks; engineered microorganisms metabolize both pentose and hexose sugars; and bioTAL yields are high. We also find that the high efficiency, low cost and low carbon intensity of PDK deconstruction and monomer recovery continue to stand out 10-22, even among emerging circular plastics 23-28. In particular, our use of TAL in place of petrochemicals in PDK production does not negatively impact PDK circularity. Instead, TAL provides an unexpected and useful bio-advantage with regard to the thermal behaviour of TAL-PDK materials, which is exploited to expand the range of serviceable applications.

BioTAL production shows promise as a bio-advantaged alternative to dimedone in the formulation of biorenewable circular PDK resins. Even moderate improvements in yield can result in costs and life cycle GHG emissions that are more competitive with the incumbent petrochemicals currently used in PDK production. However, large-scale production will require advancements along the entire supply chain to enable more efficient utilization of corn stover, including high sugar yields, the use of microbial hosts capable of metabolizing pentose and hexose sugars, and improvements in bioTAL yields. In the future, we anticipate that synthetic biology will play an increasingly important role in PDK development. PDK properties can be tailored by an interplay

of structure and chirality in monomer designs. A wide variety of structurally diverse diacids and 1,3-diketones (that is, beyond TAL) are, in principle, accessible as polyketide bioproducts, offering new targets for bioproduction (for example, by engineered polyketide synthases)⁵². Depending on the process and the feedstock required, PDK sustainability may further benefit from these carbon-negative technologies.

Methods

Synthesis of triketone monomers

Triacetic acid lactone (2.1 equivalents, or eq), carboxylic diacid (1 eq) and dimethylaminopyridine (DMAP, 3 eq) were solubilized in tetrahydrofuran on heating at 70 °C. A separate solution of dicyclohexylcarbodiimide (DCC, 2.4 eq) in tetrahydrofuran was added slowly to the reaction mixture. The reaction mixture gradually turned yellow, accompanied by the formation of a white precipitate. After the complete addition of DCC, the reaction was allowed to cool to room temperature and pursued overnight (24 h). The mixture was filtered and washed with $\mathrm{CH_2Cl_2}$ until the solid became colourless. The filtrate was concentrated and the recovered product, a dark red oil, was dissolved in $\mathrm{CH_2Cl_2}$ and extracted twice with 2.0 M HCl. The organic phase was dried over MgSO_4 and concentrated, leaving the crude product as an orange paste. The crude product was recrystallized from ethanol/water to yield yellow/orange needles.

Synthesis of PDK resins

The polymerization of PDK resins was realized using ball-milling. To the triketone monomer was added TREN, using a precalibrated micropipette such that the molar ratio of amine to triketone functional groups is 1.1:1. This was immediately followed by ball-milling the contents of the closed container for 30 min at 500 revolutions per minute (rpm) with changes in spinning direction at 1-min intervals. The reactor was opened to air and the reactor walls were scraped to bring together the reactants homogeneously. Ball-milling was resumed under identical conditions for an additional 30 min. The powders were recovered from the reactor and the residual water was removed under vacuum at 90 °C.

Acid-catalysed hydrolysis of PDK samples

PDK materials were placed in separate 40 ml vials along with 5.0 M of HCl (15 ml) and a magnetic stirrer. Depolymerization reactions were conducted over 24 h at room temperature while stirring at 500 rpm. Triketones were isolated by extraction with CH_2Cl_2 and evaporation of the organic phase.

Preparation of PDK plastics for hydrolysis

PDK resins obtained from ball-milling were compression-moulded into sheets of approximately 1 mm in thickness using a thermal press operating at 110 °C for TAL-PDK 5, 125 °C for TAL-PDK 4, 130 °C for TAL-PDK 3, 140 °C for TAL-PDK 2 and 150 °C for TAL-PDK 1, and 20,000 psi for 20 min. Small rectangular samples used for depolymerization studies were shaped with dimensions of $l=20\,$ mm, $w=5\,$ mm, $t=1\,$ mm.

Fed-batch fermentation for TAL production

The strain used for TAL production is *E. coli* JBEI-3695 harbouring plasmid pBbA5a-bktB (https://public-registry.jbei.org/entry/20892). A single colony of the strain was inoculated into 10 ml of LB medium and grown overnight at 37 °C. This seed culture (1 ml) was inoculated into LB (100 ml) in a 1-l shake flask and grown with shaking at 37 °C for 16 h, before inoculation into 1-L EZ-Rich medium (OD $_{600}$ = 0.05) in a 2-l bioreactor (Sartorius BIOSTAT B plus). Agitation, temperature, airflow and pH were maintained constant at 300 rpm, 22 °C, 0.5 volume of gas per volume of liquid per minute and pH 7.0, respectively. The culture was grown for 3–4 h at 37 °C to OD $_{600}$ = 0.6, at which point 0.1 mM of β-D-1-thiogalactopyranoside was added to the culture to induce protein production. The temperature was adjusted to 22 °C, and the culture was grown for seven days. Fed-batch experiments employed a dissolved

oxygen (DO) signal-triggered glucose feeding loop (Δ DO = 15 %, flow rate = 40 ml h⁻¹, pump duration = 5 min). Then, 1 ml cell culture was removed every 24 h for cell density and TAL titre measurement. At the end of the five-day culture, the cultures were harvested at 8,000 rpm, and TAL was extracted and purified from the supernatant.

System analysis of bioTAL production using SuperPro

The first step to conducting scenario analysis is establishing stoichiometrically maximum achievable yields. We calculated the stoichiometric maximum theoretical yield of bioTAL from glucose to be 0.7 g per g of glucose. For all four scenarios considered in this study, we assumed xylose to bioTAL conversion to be 90% of that of glucose to bioTAL conversion. The scenario associated with 'this work' reflects the bioTAL yield experimentally demonstrated in this study with glucose (14.9% of theoretical maximum yield), extrapolated to xylose assuming a commercial-scale biorefinery would use a cofermenting host. A 2.6 g l⁻¹ titre was used to calculate the yield in glucose (0.104 g per g of glucose). Then, assuming xylose to bioTAL conversion to be 90% of that of glucose to bioTAL conversion, the yield from xylose to bioTAL conversion was also calculated. A 2.6 g l-1 titre was used for the modelling purpose (instead of the highest reported titre of 2.77 g l^{-1}) as at 2.6 g l^{-1} the residence time of the bioconversion units could be kept lower, which reduces the energy use of the system, and thus lowers the MSP and the GHG emissions of the system. The intermediate and optimized scenarios are based on the assumption of achieving 50% and 90% of theoretical yield based on glucose, respectively. The 'Cao et al.' scenario is based on the bioTAL yield information obtained from article mentioned here (12.7% of theoretical maximum vield)37.

We conducted the process modelling in SuperPro Designer software⁴³. The biorefinery operates 330 days per year and 24 h per day (equivalent to 90% uptime). Capital cost accounts for equipment purchase cost, installation costs, warehouse, site development, permits, land and other field expenses and project contingency costs. Annual operating cost accounts for materials, utilities, repair and maintenance, labour and waste disposal costs. The assumptions for the model are consistent with Humbird et al. unless otherwise specified⁵³. The bulk prices for material costs were obtained from peer-reviewed literature, market price reports and Alibaba. Equipment purchase prices were derived using the built-in cost-estimating function available in SuperPro. The process parameters and assumptions for 'this work' and optimized scenarios are summarized in Supplementary Table 11. With the exception of yield, all other process parameters remained the same for 'this work' and intermediate scenarios. For the Cao et al. scenario, the same assumptions and parameters were used as that in 'this work' scenario, except during bioconversion where we used a residence time and temperature of 120 h and 30 °C, respectively, and during the recovery process, where we used crystallization to recover bioTAL instead of column chromatography³⁷.

Reporting summary

Further information on research design is available in the Nature Portfolio Reporting Summary linked to this article.

Data availability

The authors declare that the data supporting the findings of this study are available within the paper and its Supplementary Information. Crystallographic data for compounds TAL-TK 1, TAL-TK 3 and TAL-TK 5 are available free of charge from the Cambridge Crystallographic Data Centre (www.ccdc.cam.ac.uk) under reference numbers 2223455, 2223456 and 2223457, respectively.

References

 Rosenboom, J.-G., Langer, R. & Traverso, G. Bioplastics for a circular economy. Nat. Rev. Mater. 7, 117–137 (2022).

- Kakadellis, S. & Rosetto, G. Achieving a circular bioeconomy for plastics. Science 373, 49–50 (2021).
- Fagnani, D. E. et al. 100th anniversary of macromolecular science viewpoint: redefining sustainable polymers. ACS Macro Lett. 10, 41–53 (2021).
- 4. Haque, F. M. et al. Defining the macromolecules of tomorrow through synergistic sustainable polymer research. *Chem. Rev.* **122**, 6322–6373 (2022).
- Kawaguchi, H., Ogino, C. & Kondo, A. Microbial conversion of biomass into bio-based polymers. *Bioresour. Technol.* 245, 1664–1673 (2017).
- Cywar, R. M., Rorrer, N. A., Hoyt, C. B., Beckham, G. T. & Chen, E. Y.-X. Bio-based polymers with performance-advantaged properties. Nat. Rev. Mater. 7, 83–103 (2022).
- Coates, G. W. & Getzler, Y. D. Y. L. Chemical recycling to monomer for an ideal, circular polymer economy. *Nat. Rev. Mater.* 5, 501–516 (2020).
- 8. Borrelle, S. B. et al. Predicted growth in plastic waste exceeds efforts to mitigate plastic pollution. *Science* **369**, 1515–1518 (2020).
- 9. von Vacano, B. et al. Sustainable design of structural and functional polymers for a circular economy. *Angew. Chem. Int. Ed.* **62**, e202210823 (2022).
- Haeussler, M., Eck, M., Rothauer, D. & Mecking, S. Closed-loop recycling of polyethylene-like materials. *Nature* 590, 423–427 (2021).
- Abel, B. A., Snyder, R. L. & Coates, G. W. Chemically recyclable thermoplastics from reversible-deactivation polymerization of cyclic acetals. Science 373, 783–789 (2021).
- Rapagnani, R. M., Dunscomb, R. J., Fresh, A. A. & Tonks, I. A. Tunable and recyclable polyesters from CO₂ and butadiene. *Nat. Chem.* 14, 877–883 (2022).
- 13. Zhu, J.-B., Watson, E. M., Tang, J. & Chen, E. Y.-X. A synthetic polymer system with repeatable chemical recyclability. *Science* **360**, 398–403 (2018).
- Hong, M. & Chen, E. Y.-X. Completely recyclable biopolymers with linear and cyclic topologies via ring-opening polymerization of y-butyrolactone. *Nat. Chem.* 8, 42–49 (2016).
- Cywar, R. M. et al. Redesigned hybrid nylons with optical clarity and chemical recyclability. J. Am. Chem. Soc. 144, 5366–5376 (2022).
- Yuan, P., Sun, Y., Xu, X., Luo, Y. & Hong, M. Towards high-performance sustainable polymers via isomerization-driven irreversible ring-opening polymerization of five-membered thionolactones. *Nat. Chem.* 14, 294–303 (2022).
- Lei, Z. et al. Recyclable and malleable thermosets enabled by activating dormant dynamic linkages. *Nat. Chem.* 14, 1399–1404 (2022).
- Mohadjer Beromi, M. et al. Iron-catalysed synthesis and chemical recycling of telechelic 1,3-enchained oligocyclobutanes. *Nat. Chem.* 13, 156–162 (2021).
- Zhang, Z. et al. Strong and tough supramolecular covalent adaptable networks with room-temperature closed-loop recyclability. Adv. Mater. 35, 2208619 (2022).
- Sullivan, K. P. et al. Mixed plastics waste valorization through tandem chemical oxidation and biological funneling. Science 378, 207–211 (2022).
- Saito, K., Eisenreich, F., Tuerel, T. & Tomovic, Z. Closed-loop recycling of poly(imine-carbonate) derived from plastic waste and bio-based resources. *Angew. Chem. Int. Ed.* 61, e202211806 (2022).
- 22. Li, Z., Zhao, D., Shen, Y. & Li, Z. Ring-opening polymerization of enantiopure bicyclic ether-ester monomers toward closed-loop recyclable and crystalline stereoregular polyesters via chemical upcycling of bioplastic. *Angew. Chem. Int. Ed.* **62**, e202302101 (2023).

- Christensen, P. R., Scheuermann, A. M., Loeffler, K. E. & Helms, B. A. Closed-loop recycling of plastics enabled by dynamic covalent diketoenamine bonds. *Nat. Chem.* 11, 442–448 (2019).
- He, C. et al. Conformational entropy as a means to control the behavior of poly(diketoenamine) vitrimers in and out of equilibrium. *Angew. Chem. Int. Ed.* 59, 735–739 (2020).
- 25. Vora, N. et al. Leveling the cost and carbon footprint of circular polymers that are chemically recycled to monomer. *Sci. Adv.* **7**, eabf0187 (2022).
- Demarteau, J., Vora, N., Keasling, J. D., Helms, B. A. & Scown, C. D. Lower-cost, lower-carbon production of circular polydiketoenamine plastics. ACS Sustain. Chem. Eng. 10, 2740–2749 (2022).
- Demarteau, J. et al. Circularity in mixed-plastic chemical recycling enabled by variable rates of polydiketoenamine hydrolysis.
 Sci. Adv. 8, eabp8823 (2022).
- 28. Helms, B. A. Polydiketoenamines for a circular plastics economy. Acc. Chem. Res. **55**, 2753–2765 (2022).
- Vermeulen, I., Van Caneghem, J., Block, C., Baeyens, J. & Vandecasteele, C. Automotive shredder residue (ASR): reviewing its production from end-of-life vehicles (ELVs) and its recycling, energy or chemicals' valorization. J. Hazard. Mater. 190, 8–27 (2011).
- Denissen, W., Winne, J. M. & Du Prez, F. E. Vitrimers: permanent organic networks with glass-like fluidity. *Chem. Sci.* 7, 30–38 (2016).
- Jin, Y., Lei, Z., Taynton, P., Huang, S. & Zhang, W. Malleable and recyclable thermosets: the next generation of plastics. *Matter* 1, 1456–1493 (2019).
- 32. Scheutz, G. M., Lessard, J. J., Sims, M. B. & Sumerlin, B. S. Adaptable crosslinks in polymeric materials: resolving the intersection of thermoplastics and thermosets. *J. Am. Chem. Soc.* **141**, 16181–16196 (2019).
- Wang, R., Johnson, J. A. & Olsen, B. D. Odd-even effect of junction functionality on the topology and elasticity of polymer networks. *Macromolecules* 50, 2556–2564 (2017).
- Coffman, D. D., Berchet, G. J., Peterson, W. R. & Spanagel, E. W. Polymeric amides from diamines and dibasic acids. *J. Polym. Sci.* 2, 306–313 (1947).
- Rimando, A. & Baerson, S. Polyketides: biosynthesis, biological activity, and genetic engineering. *Polyketides (ACS Symp. Ser.)* 955. 1–5 (2007).
- 36. Markham, K. A. et al. Rewiring *Yarrowia lipolytica* toward triacetic acid lactone for materials generation. *Proc. Natl Acad. Sci. USA* **115**, 2096–2101 (2018).
- Cao, M. et al. Metabolic engineering of oleaginous yeast Rhodotorula toruloides for overproduction of triacetic acid lactone. Biotechnol. Bioeng. 119, 2529–2540 (2022).
- Tan, Z., Clomburg, J. M., Cheong, S., Qian, S. & Gonzalez, R. A polyketoacyl-CoA thiolase-dependent pathway for the synthesis of polyketide backbones. *Nat. Catal.* 3, 593–603 (2020).
- 39. Wang, Z. et al. A highly active *Burkholderia* polyketoacyl-CoA thiolase for production of triacetic acid lactone. Preprint at *bioRxiv* https://doi.org/10.1101/2022.12.04.519061 (2022).
- Sierra-Ibarra, E. et al. Ethanol production by Escherichia coli from detoxified lignocellulosic teak wood hydrolysates with high concentration of phenolic compounds. J. Ind. Microbiol. Biotechnol. 49, kuab077 (2022).
- Tang, S.-Y. et al. Screening for enhanced triacetic acid lactone production by recombinant *Escherichia coli* expressing a designed triacetic acid lactone reporter. *J. Am. Chem. Soc.* 135, 10099–10103 (2013).
- 42. Xie, D. et al. Microbial synthesis of triacetic acid lactone. Biotechnol. Bioeng. **93**, 727–736 (2006).

- 43. SuperPro Designer (Intelligen, Inc., 2014).
- 44. Alibaba.com (accessed September 2022); https://www. alibaba.com/product-detail/CAS-126-81-8-Dimedone-C8H12O2_1600455883706.html?spm=a2700.7724857.0.0.79e37b 39MEK2Ha
- 45. Alibaba.com (accessed February 2023); (a) https://www.alibaba.com/product-detail/Granules-Hdpe-Factory-Price-Pipe-Grade_1600284744902.html?spm=a2700.galleryofferlist.0.0.142 858bcBUPNVJ; (b) https://www.alibaba.com/product-detail/High-Quality-China-Manufacture-Foaming-Agent_1600661087016.ht ml?spm=a2700.7724857.0.0.60448b57efKUZa&s=p; (c) https://www.alibaba.com/product-detail/Pet-Resin-Polyethylene-Terephthalate-Plastic-Raw_1600190831818.html?spm=a2700.details.0.0.67cd6493D58qSL
- Amelio, A., Genduso, G., Vreysen, S., Luis, P. & der Bruggen, B. Guidelines based on life cycle assessment for solvent selection during the process design and evaluation of treatment alternatives. *Green. Chem.* 16, 3045–3063 (2014).
- 47. Kyulavska, M., Toncheva-Moncheva, N. & Rydz, J. Biobased polyamide ecomaterials and their susceptibility to biodegradation. in *Handbook of Ecomaterials* (eds Martínez, L. et al.) 1–34 (Springer, Cham., 2017).
- 48. Wernet, G. et al. The ecoinvent database version 3 (part I): overview and methodology. *Int. J. Life Cycle Assess.* **21**, 1218–1230 (2016).
- 49. U.S. Life Cycle Inventory Database (National Renewable Energy Laboratory, 2012); http://www.nrel.gov/lci/
- Wang, M. The Greenhouse Gases, Regulated Emissions, and Energy Use in Transportation (GREET) Model: Version 1.5 (Center for Transportation Research, Argonne National Laboratory, 2008); http://eng.sut.ac.th/transportenergy/data/ paper4web/The%20GHG%20regulated%20emission%20 and%20energy%20use%20in%20transportation%20model% 20-%2099.pdf
- Waste reduction model. US Environmental Protection Agency https://www.epa.gov/warm/versions-waste-reduction-modelwarm#15 (2010).
- Huang, Y., Hoefgen, S., Gherlone, F. & Valiante, V. Intrinsic ability of the β-oxidation pathway to produce bioactive styrylpyrones. Angew. Chem. Int. Ed. 61, e202206851 (2022).
- Humbird, D. et al. Process Design and Economics for Biochemical Conversion of Lignocellulosic Biomass to Ethanol: Dilute-Acid Pretreatment and Enzymatic Hydrolysis of Corn Stover (US Department of Energy, 2011); http://www.osti.gov/servlets/ purl/1013269-rQta8H/

Acknowledgements

We acknowledge support from the United States Department of Energy (DOE) Bioenergy Technologies Office award no. 1916-1597. Portions of this work—including polymer synthesis, recycling and characterization—were carried out as a User Project at the Molecular Foundry, which is supported by the Office of Science, Office of Basic Energy Sciences, of the DOE under contract no. DE-ACO2-05CH11231. This work was supported by the Joint BioEnergy Institute (https://www.jbei.org), which is supported by the DOE, Office of Science, Office of Biological and Environmental Research under contract no. DE-ACO2-05CH11231. The Solid-State NMR instrument used in this work is supported by the National Science Foundation under grant no. 2018784. This research used resources of the Advanced Light Source, which is a DOE Office of Science User Facility under contract no. DE-AC02-05CH11231. We thank A. Lund for her help with the solid-state NMR data acquisition. We thank S. L. Nordahl for helpful discussions on LCA analysis.

Author contributions

All authors contributed to the conceptualization of the project. J.D., B.C. and B.A.H. contributed the methodology for polymer design and chemical recycling. B.B., N.R.B. and C.D.S. contributed the methodology for systems analysis. Z.W., S.C., G.L. and J.D.K. contributed the methodology for bioTAL production. S.J.T. contributed the methodology for monomer characterization by X-ray diffraction. All authors contributed to analysing the data. B.A.H., J.D., Z.W. and B.B. wrote the original draft. All authors contributed to writing the final draft and editing. B.A.H. and J.D. contributed to visualization. B.A.H. supervised the research. J.D.K., C.D.S. and B.A.H. provided project administration. J.D.K., C.D.S. and B.A.H. acquired funding.

Competing interests

The authors declare the following competing interests: B.A.H. is an inventor on the US provisional patent application 62/587,148 submitted by Lawrence Berkeley National Laboratory that covers PDKs, as well as aspects of their use and recovery. B.A.H., J.D. and J.D.K. are inventors on the US provisional patent application 63/390,962 submitted by Lawrence Berkeley National Laboratory that covers TAL-PDKs, as well as aspects of their use and recovery. J.D.K. has a financial interest in Amyris, Lygos, Demetrix, Napigen, Maple Bio, Apertor Labs, Berkeley Yeast, Ansa Biotechnologies and Zero Acre Farms. B.A.H., J.D.K. and C.D.S. have a financial interest in Cyklos Materials. The remaining authors declare no competing interests.

Additional information

Supplementary information The online version contains supplementary material available at https://doi.org/10.1038/s41893-023-01160-2.

Correspondence and requests for materials should be addressed to Brett A. Helms.

Peer review information *Nature Sustainability* thanks Haritz Sardon, Tomonori Saito and the other, anonymous, reviewer(s) for their contribution to the peer review of this work.

Reprints and permissions information is available at www.nature.com/reprints.

Publisher's note Springer Nature remains neutral with regard to jurisdictional claims in published maps and institutional affiliations.

Springer Nature or its licensor (e.g. a society or other partner) holds exclusive rights to this article under a publishing agreement with the author(s) or other rightsholder(s); author self-archiving of the accepted manuscript version of this article is solely governed by the terms of such publishing agreement and applicable law.

© The Author(s), under exclusive licence to Springer Nature Limited 2023

nature portfolio

Corresponding author(s):	Brett A. Helms
Last updated by author(s):	Dec 16, 2022

Reporting Summary

Nature Portfolio wishes to improve the reproducibility of the work that we publish. This form provides structure for consistency and transparency in reporting. For further information on Nature Portfolio policies, see our <u>Editorial Policies</u> and the <u>Editorial Policy Checklist</u>.

For all statistical analyses, confirm that the following items are present in the figure legend, table legend, main text, or Methods section.

<u> </u>			
St	·at	ıstı	100

n/a	Confirmed
	$oxed{\boxtimes}$ The exact sample size (n) for each experimental group/condition, given as a discrete number and unit of measurement
	🔀 A statement on whether measurements were taken from distinct samples or whether the same sample was measured repeatedly
\boxtimes	The statistical test(s) used AND whether they are one- or two-sided Only common tests should be described solely by name; describe more complex techniques in the Methods section.
\boxtimes	A description of all covariates tested
\boxtimes	A description of any assumptions or corrections, such as tests of normality and adjustment for multiple comparisons
	A full description of the statistical parameters including central tendency (e.g. means) or other basic estimates (e.g. regression coefficient) AND variation (e.g. standard deviation) or associated estimates of uncertainty (e.g. confidence intervals)
	For null hypothesis testing, the test statistic (e.g. <i>F</i> , <i>t</i> , <i>r</i>) with confidence intervals, effect sizes, degrees of freedom and <i>P</i> value noted <i>Give P values as exact values whenever suitable.</i>
\boxtimes	For Bayesian analysis, information on the choice of priors and Markov chain Monte Carlo settings
\boxtimes	For hierarchical and complex designs, identification of the appropriate level for tests and full reporting of outcomes
\boxtimes	Estimates of effect sizes (e.g. Cohen's <i>d</i> , Pearson's <i>r</i>), indicating how they were calculated
	Our web collection on statistics for biologists contains articles on many of the points above.

Software and code

Policy information about availability of computer code

Data collection

We obtained life-cycle inventory data and characterization factors for input materials and commodity polymers from peer-reviewed literature, and LCA databases including Ecoinvent, US Life Cycle Inventory (USLCI), GREET, and WARM models. We measured the cell growth on SpectraMax M2. We quantified of triacetic acid lactone (TAL) on Agilent HPLC system with a DAD (G1315D) and a reverse phase column (Kinetex 5 µm EVO C18, 150X4.6 mm). We purified TAL on CombiFlash NEXTGEN 300+ with a silica column (RediSep, Cat. 69-2203-349).

Data analysis

We conducted the process modeling in SuperPro Designer software. We analyzed the data of TAL production in Agilent Chemstation software.

For manuscripts utilizing custom algorithms or software that are central to the research but not yet described in published literature, software must be made available to editors and reviewers. We strongly encourage code deposition in a community repository (e.g. GitHub). See the Nature Portfolio guidelines for submitting code & software for further information.

Data

Policy information about availability of data

All manuscripts must include a data availability statement. This statement should provide the following information, where applicable:

- Accession codes, unique identifiers, or web links for publicly available datasets
- A description of any restrictions on data availability
- For clinical datasets or third party data, please ensure that the statement adheres to our policy

The authors declare that the data supporting the findings of this study are available within the paper and its Supplementary Information, and also available from the

Centre (www.ccdc.car	m.ac.uk) under	ic data for compounds TAL-TK 1, TAL-TK 3 and TAL-TK 5 are available free of charge from the Cambridge Crystallographic Date reference numbers 2223455, 2223456 and 2223457, respectively. The strain used in this study is available from the all transfer agreement.		
Human resea	arch parti	cipants		
Policy information a	bout <u>studies i</u>	nvolving human research participants and Sex and Gender in Research.		
Reporting on sex and gender N/A		N/A		
Population charac	cteristics	N/A		
Recruitment		N/A		
Ethics oversight		N/A		
		oval of the study protocol must also be provided in the manuscript.		
Field-spe				
		s the best fit for your research. If you are not sure, read the appropriate sections before making your selection.		
Life sciences		Behavioural & social sciences		
Life scien	ces sti	udy design		
All studies must disclose on these points even when the disclosure is negative.				
Sample size	Sample size of	three or more was taken.		
Data exclusions	No data was ex	cluded in the processing of data analysis.		
Replication The fermentation experiments were performed with two replicates.		on experiments were performed with two replicates.		
Randomization The engineered strain was randomly picked up from the agar plate.		d strain was randomly picked up from the agar plate.		
Blinding	The analytical §	group who analyzed the data were blind to the samples being analyzed.		
We require information system or method listed Materials & exp n/a Involved in the	on from authors ed is relevant to perimental s	n/a Involved in the study		
Antibodies		ChIP-seq		
Eukaryotic cell lines Palaeontology and archaeology		logy Flow cytometry MRI-based neuroimaging		
Animals and other organisms				
Clinical data				
Dual use research of concern				